AIAA JOURNAL
Vol. 34, No. 5, May 1996

Calculation of the Radiated Sound Field Using an Open Kirchhoff Surface

Jonathan B. Freund,* Sanjiva K. Lele,† and Parviz Moin‡
Stanford University, Stanford, California 94305

Means of improving the accuracy of Kirchhoff surface-integral evaluations for sound fields in cases where the surface may not be completely closed are investigated. Asymptotic analysis for large temporal wave number is used to analyze time-harmonic integral forms. Applicability to the moderate temporal wave numbers of real problems is discussed. Stationary-phase arguments are used to show geometrically where good results are expected from a Kirchhoff integral on an open surface. A similar asymptotic analysis is used to provide correction terms to account partially for the missing portion of the integral surface. The present study is restricted to the case where the mean flow is parallel to the available portion of the surface. The analysis is extended to time-domain formulation of transient problems. Two- and three-dimensional numerical examples are given to demonstrate and evaluate the method. It is found that the derived correction terms can reduce the error in an open-surface calculation of the radiated sound field by more than an order of magnitude.

Nomenclature

c	= sound speed
F	= integrand amplitude in asymptotic analysis
G	= Green's function for wave operator
$H_n^{(2)}$	= Hankel function, order n, second kind
k	= temporal wave number, ω/c.
L	= length of available Kirchhoff surface
M	= mean-flow Mach number (in x_1 direction)
S	= virtual acoustic source
t	= time
$\boldsymbol{x}$	= listener point in space
$\boldsymbol{y}$	= Kirchhoff-surface point in space
$\boldsymbol{z}$	= acoustic-source point in space
$\delta(\boldsymbol{x})$	= Dirac delta evaluated at $\boldsymbol{x}$
$\partial\Omega_K$	= Kirchhoff surface
ϕ	= acoustic field variable
ψ	= integrand phase in asymptotic analysis
Ω_S	= acoustic-source volume
ω	= temporal angular frequency

I. Introduction

THE Kirchhoff-surface technique is becoming a familiar tool in computational acoustics (see Lyrintzis[1] for a review of studies involving Kirchhoff formulations). The primary application of concern in this study is the calculation of an acoustic far field from near-field data taken from an unsteady-compressible-flow calculation. The method utilizes surface integrals that are derived from linear free-space wave propagation problems in conjunction with the Sommerfeld radiation condition. The integrals are evaluated on an arbitrary surface enclosing a source region. These formulas have been known for more than 100 years,[2] but it is only recently that computers and techniques have become advanced enough to solve accurately for the source field and the near acoustic field in an aerodynamic sound-generation study. A Kirchhoff-integral technique may be used in conjunction with such a near-field calculation to efficiently calculate the far-field radiated sound at any point exterior to the surface, thus avoiding the computational expense of carrying the source-region calculation into the far acoustic field. An acoustic variable such as pressure or dilatation is defined on the surface by the source-region calculation of a flow such as a jet or mixing layer, and a surface-integral evaluation then gives the acoustic field beyond that surface. It is important that the surface be placed so that it lies beyond any nonlinear or viscous source-region effects. Essentially, the surface must be placed in a region where the flow is completely governed by a homogeneous linear wave equation with constant coefficients, for which there exists a free-space Green's function.

However, in the case of mixing layers or jets there is the difficulty that the hydrodynamic source region decays very slowly in the downstream direction. Artificial boundary conditions are necessarily imposed at the outflow (and often the inflow) domain boundaries to maintain a manageable size for the source-region calculation. Unfortunately, at these boundaries it is impossible to separate out the acoustic portion of the flow for use in the Kirchhoff integrand, as the flow here is governed by the full viscous, heat conducting, nonlinear equations. (See Fig. 1.) The Kirchhoff surface may not then be closed. For a Kirchhoff-integral evaluation to be an exact representation of the sound field, it is required that acoustic data be available on a surface completely enclosing all acoustic sources. For flows with persistent downstream hydrodynamics, there no longer exists an exact Kirchhoff formulation for a finite-sized surface. The missing portion must be left out (as by Mitchell et al.[3] and Lyrintzis and Mankbadi[4]) or modeled. The common practice has been to leave the unavailable portion of the near-field acoustic data out of the evaluation. This is equivalent to dictating that the acoustic variable as well as its normal derivative is uniformly zero on the missing portion of the surface. That is unphysical, and a study of when it is justified in such a calculation is needed.

This paper will offer justification and correction for the present practice of zeroing the unavailable portion of the acoustic data. Section II will formulate frequency-domain Kirchhoff integral equations for their evaluation and analysis. Section III will examine

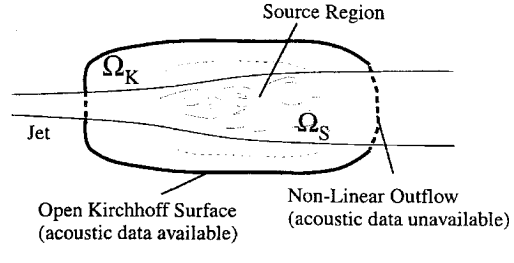

Fig. 1 Schematic showing where acoustic data become unavailable in a jet noise measurement or calculation.

Received Aug. 12, 1995; revision received Nov. 29, 1995; accepted for publication Dec. 18, 1995.

*Research Assistant, Department of Mechanical Engineering.
†Assistant Professor, Department of Mechanical Engineering and Department of Aeronautics and Astronautics. Member AIAA.
‡Franklin and Caroline Johnson Professor of Engineering, Department of Mechanical Engineering; also Senior Staff Scientist, NASA Ames Research Center, Moffett Field, CA 94035. Associate Fellow AIAA.

the asymptotic behavior of the integrals using the nondimensional temporal wave number $kL = \omega L/c$ as a large parameter and will offer a justification for zeroing the unavailable portions of the near-field acoustic data when calculating certain regions of the far field. An asymptotic correction to the open integral will be given, and sample calculations will show its effectiveness even for the finite temporal wave numbers of real sound-generation studies. We extend the analysis to problems formulated in the time domain in Sec. IV. A transient radiation problem is used to demonstrate the effectiveness of the corrections terms.

II. Formulation

The standard Kirchhoff-integral solution for a harmonic wave field is[5]

$$\phi(\boldsymbol{x}) = \int_{\partial\Omega_K} [\phi(\boldsymbol{y})G_n(\boldsymbol{x}-\boldsymbol{y}) - \phi_n(\boldsymbol{y})G(\boldsymbol{x}-\boldsymbol{y})]\,\mathrm{d}S(\boldsymbol{y}) \tag{1}$$

Subscript n indicates partial differentiation in the direction of the outward-pointing normal to the surface (e.g., $\phi_n = \boldsymbol{n}\cdot\nabla\phi$). It is assumed that $\phi(\boldsymbol{y})$ and $\phi_n(\boldsymbol{y})$ are known with sufficient accuracy on $\boldsymbol{y} \in \partial\Omega_K$. This assumption is justified by the argument that if the near-field source calculation is assumed to be accurate enough to resolve the near acoustic field, we must necessarily have accurate data on the Kirchhoff surface and have the resolution necessary to calculate normal derivatives of the data on that surface. Ω_K is the region bounded by $\partial\Omega_K$, and Eq. (1) predicts the sound in Ω_K^C, the region exterior to $\partial\Omega_K$. In Eq. (1), $\boldsymbol{x}$ is any point in space such that $\boldsymbol{x} \notin \partial\Omega_K$; however, the solution for $\boldsymbol{x} \in \Omega_K$ is uniformly zero by the nature of the integrals.[6] G is the free-space Green's function of the wave operator governing the acoustic region. We consider the reduced wave equation, and G then is the solution to

$$(\Delta + k^2)G = \delta(\boldsymbol{x}) \tag{2}$$

where Δ is the Laplace operator. If the temporal dependence is taken to be $\exp(+i\omega t)$, then the free-space Green's function has the following form in two and three dimensions, respectively:

$$G(\boldsymbol{x}) = \frac{1}{4i}H_0^{(2)}(k|\boldsymbol{x}|), \qquad G(\boldsymbol{x}) = \frac{1}{4\pi|\boldsymbol{x}|}\exp(-ik|\boldsymbol{x}|) \tag{3}$$

For $k|\boldsymbol{x}| \to \infty$ there exists a uniform asymptotic solution[7] for a general number of dimensions d:

$$G(\boldsymbol{x}) \sim \frac{1}{2ik}\left(\frac{k}{2\pi|\boldsymbol{x}|}\right)^{(d-1)/2}\exp\left[i(d-1)\frac{\pi}{4}\right]\exp(-ik|\boldsymbol{x}|) \tag{4}$$

This relation is exact for any $k|\boldsymbol{x}|$ if $d = 1$ or 3. We note that the phase of the solution is the same function of $k|\boldsymbol{x}|$ regardless of the problem's spatial dimension, and we will take advantage of this to add generality to the results.

When there exists a uniform mean flow, we use the free-space Green's function of the convected reduced wave equation

$$\left(\Delta - M^2\frac{\partial^2}{\partial x_1^2} - 2ikM\frac{\partial}{\partial x_1} + k^2\right)\phi = 0 \tag{5}$$

The Green's function in two dimensions is

$$G(\boldsymbol{x}) = \frac{\exp[ix_1kM/(1-M^2)]}{4i\sqrt{1-M^2}} \times H_0^{(2)}\left[\sqrt{\frac{x_1^2}{1-M^2}+x_2^2}\left(\frac{1}{1-M^2}\right)^{\frac{1}{2}}k\right] \tag{6}$$

M is the mean-flow Mach number, and the mean flow is in the x_1 direction. A similar solution exists for the case of three spatial dimensions. This free-space Green's function has been used by Wu and Lee[8] in formulating boundary integral formulas, and asymptotic forms of a more general solution have been used by Howe.[9] The integral formulation, derived by the methods of Farassat and Myers[10] for the convected form of the equation, is

$$\phi(\boldsymbol{x}) = \int_{\partial\Omega_K} [\nabla\phi\cdot\boldsymbol{N}G - \phi\boldsymbol{N}\cdot\nabla G - 2ikM\phi n_1 G]\,\mathrm{d}S(\boldsymbol{y}) \tag{7}$$

The acoustic variable ϕ is evaluated at $\boldsymbol{y}$, and the fundamental solution G [defined in Eq. (6)] is evaluated at $\boldsymbol{x}-\boldsymbol{y}$. Here $\boldsymbol{N}$ is a modified surface normal $\boldsymbol{N} = \langle(1-M^2)n_1, n_2\rangle$, where $\langle n_1, n_2\rangle$ is the true surface normal. This formulation easily reduces to the form of Eq. (1) in the case where the mean flow is parallel to the surface ($n_1 = 0$). Most of the following analyses will consider the case $M = 0$ to simplify the algebraic presentation of the results. All the following applies directly to subsonic M parallel to the surface, and some sample calculations for subsonic $M > 0$, $n_1 = 0$ are included in this paper.

In the following analyses we will be concerned with the spatial phase of the integrands. This phase is not explicitly given in Eq. (1) even upon substitution of asymptotic forms of the Green's function (4), because it is partly contained within the ϕ and ϕ_n terms. We may extract the phase by assuming that there exists a source field $\mathcal{S}(\boldsymbol{x})$ giving rise to the acoustic field on $\partial\Omega_K$. Our Kirchhoff method prescribes that $\mathcal{S}$ has compact support in some region $\Omega_S \subset \Omega_K$ (see Fig. 1). We still assume that the hydrodynamics of the source flow persist downstream of Ω_K, making acoustic data unavailable, but that this persistent flow does not contribute to the sound radiation of interest. It is not required that $\mathcal{S}$ be unique, as it will only be used as an intermediate variable and not be present in final results. $\mathcal{S}$ may also contain equivalent sources for any reflecting surfaces in Ω_S. The field may then be represented by

$$\phi(\boldsymbol{y}) = \int_{z\in\Omega_S} \mathcal{S}(z)G(\boldsymbol{y}-\boldsymbol{z})\,\mathrm{d}z \tag{8}$$

and the Kirchhoff integral becomes

$$\phi(\boldsymbol{x}) = \int_{z\in\Omega_S}\int_{y\in\partial\Omega_K} \mathcal{S}(z)[G_n(\boldsymbol{y}-\boldsymbol{z})G(\boldsymbol{x}-\boldsymbol{y}) - G(\boldsymbol{y}-\boldsymbol{z})G_n(\boldsymbol{x}-\boldsymbol{y})]\,\mathrm{d}S(\boldsymbol{y})\,\mathrm{d}z \tag{9}$$

This equation may be rewritten with the spatial phase explicit in the integrand:

$$\phi(\boldsymbol{x}) = \int_{z\in\Omega_S}\int_{y\in\partial\Omega_K} F(\boldsymbol{y},\boldsymbol{z},\boldsymbol{x})\exp[-ik\psi(\boldsymbol{y},\boldsymbol{z},\boldsymbol{x})]\,\mathrm{d}S(\boldsymbol{y})\,\mathrm{d}z \tag{10}$$

In two spatial dimensions the asymptotic form of the fundamental solution as given in Eq. (4) is used to write the phase term explicitly, and the $=$ in Eq. (10) should be replaced by a $\sim$ for formality. The phase is simply

$$\psi(\boldsymbol{y},\boldsymbol{z},\boldsymbol{x}) = |\boldsymbol{x}-\boldsymbol{y}| + |\boldsymbol{y}-\boldsymbol{z}| \tag{11}$$

The explicit form of F is easily derived, but is dependent on the problem under consideration and will not be needed in much of the following. We proceed taking F as a known function on the available portion of $\partial\Omega_K$.

We complete our formulation by choosing a specific geometry for $\partial\Omega_K$ appropriate for a two- or three-dimensional jet or mixing layer. The chosen surface spans the computational box in the streamwise direction at a constant distance h from the centerline of the flow. The centerline is used as an arbitrary reference point for the coordinate system. A surface appropriate for the three-dimensional jet is presented graphically in Fig. 2. The surface extends from location (a, h) on the inflow boundary to location (b, h) on the outflow boundary and azimuthally around the jet to form a circular cylinder. A two-dimensional flow will have only two lines extending from point a to point b at $\pm h$, and a three-dimensional mixing layer will have surfaces extending over the width of the computational domain at $\pm h$, a periodic direction in most computations. The upstream and downstream ends of the boundary (the two ends of the cylinder in Fig. 2) are assumed not to have acoustic data available for use and thus represent the unclosable portion of the surface. In the

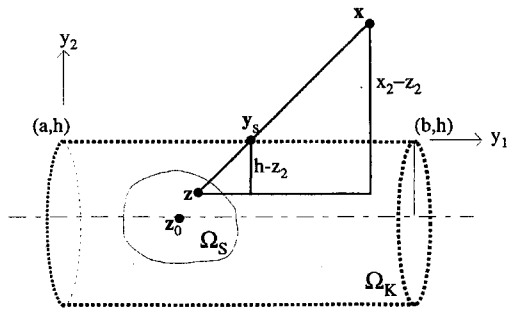

Fig. 2 Diagram of the particular surface used for analysis. Here x is the observation point, $y_s = (y_{1s}, h)$ is the stationary point, and Ω_S is the source region with source coordinates $z = (z_1, z_2)$.

three-dimensional cases it is assumed that the θ- or y_3-direction integration on Ω_K may be handled accurately without difficulty using any standard or spectral method.

We now explicitly show the $\partial\Omega_K$ integration for the jet geometry pictured in Fig. 2 including the three dimensionality:

$$\phi(\boldsymbol{x}) = \int_{z\in\Omega_S}\int_0^{2\pi}\left[\int_a^b F(y_1; h, \theta, \boldsymbol{z}, \boldsymbol{x}) \times \exp[-ik\psi(y_1; h, \theta, \boldsymbol{z}, \boldsymbol{x})]\,dy_1\right] d\theta\,dz \tag{12}$$

The outer integrals on Ω_S and θ are considered to be exact, and the inner integral, contained within the brackets, represents the breakdown of Kirchhoff formality because the surface is not closed. The exact integral would span the infinite domain $(-\infty, \infty)$ or include end surfaces. The following analyses will deal with this inner integral. The semicolon has been introduced into the arguments of F and ψ to separate the variable of integration in the inner integral, y_1, from the variables h, θ, $\boldsymbol{z}$, and $\boldsymbol{x}$, which will be considered constant parameters in much of the following.

III. Asymptotic Analysis

We will now analyze the innermost integral of Eq. (12). We take k to be a large parameter for the analysis. When it is correctly normalized by L (the domain size in y_1), the resulting product kL is found, depending upon the frequency under consideration, to be larger than about 10 in computations of interest (see, for example, computations of Colonius et al.[11] and Mitchell et al.[3]). This corresponds to having a few wavelengths per domain length. Though this value might not seem large, we note that we will not rely on the asymptotic solution itself, but will rather be guided by the asymptotic analysis to justify the use of open surfaces and make corrections to open-surface calculations. The major portion of any solution will still come from numerical quadrature of the integral in question, and thus we proceed allowing for merely moderate values of kL. In the following discussions L is taken to be a constant. Therefore trends in kL and trends in k are analogous, and $\mathcal{O}[(kL)^n]$ behavior is equivalent to $\mathcal{O}(k^n)$ behavior.

A. Stationary-Phase Justification of Open Surfaces

We begin our analysis of the innermost integral in Eq. (12) by considering a closed integral that is infinite in the y_1 direction:

$$I = \int_{-\infty}^{\infty} F(y_1)\exp[-ik\psi(y_1)]\,dy_1 \tag{13}$$

When the range of integration is extended to infinity upstream and downstream ($a = -\infty$, $b = +\infty$), Eq. (12) again becomes formally exact. In two dimensions this infinite extension also accounts for the line integration at $y_2 = -h$, and the following will also show why that portion of the integral need not be included in evaluation for sound-field points with $x_2 > h$. We now analyze this integral to see if the major contribution to it comes from the region $[a, b]$ on which we have data available. Analysis proceeds by the method of stationary phase. The stationary-phase argument is as follows. Since k is large, the integrand is rapidly oscillating except at points where $\psi(y_1)$ is slowly varying. This occurs in the neighborhood of stationary points y_{1s} defined by

$$\psi'(y_{1s}) = 0 \tag{14}$$

Away from stationary points, the rapid oscillations of the integrand tend to cancel each other and yield no net contribution to the value of the integral.

We may solve for the stationary point by taking the y_1 derivative of ψ:

$$\psi'(y_1; y_2, z, \boldsymbol{x}) = \frac{y_1 - z_1}{|\boldsymbol{y} - \boldsymbol{z}|} - \frac{x_1 - y_1}{|\boldsymbol{x} - \boldsymbol{y}|} = 0 \tag{15}$$

This equation is best analyzed geometrically as pictured in Fig. 2. Arguments stemming from similar-triangle relationships may be used to derive the following explicit expression for y_{1s}:

$$y_{1s} = z_1 + (h - z_2)\frac{x_1 - z_1}{x_2 - z_2} \tag{16}$$

This is the point of intersection between the Kirchhoff surface and a line extending between the source point $\boldsymbol{z}$ and the observation location $\boldsymbol{x}$. This geometrical relation also holds exactly in the case when the mean flow is subsonic and parallel to the y_1 direction. We now have definite bounds on $\boldsymbol{x}$ locations such that the major contribution of the exact infinite integral in Eq. (13) also lies on the available portion of the surface $y_1 \in [a, b]$. This is a result of our definition of Ω_S requiring that it be contained within Ω_K: it is guaranteed that if $x_1 \in [a, b]$, then the stationary point lies in $[a, b]$ and we are able to numerically calculate the dominant contribution to the integral in the asymptotic limit of $k \to \infty$.

Expanding ψ and F about the stationary point in Taylor series, we may calculate the asymptotic value of the integral. It is

$$I \sim \exp[-ik\psi(y_{1s})]F(y_{1s})\exp\left[-\frac{i\pi}{4}\frac{\psi''(y_{1s})}{|\psi''(y_{1s})|}\right]\sqrt{\frac{2\pi}{k|\psi''(y_{1s})|}} \qquad k\to\infty \tag{17}$$

which has a $F/\sqrt{k}$ asymptotic dependence. A similar asymptotic solution was used by Lax and Feshbach[12] to calculate scattering in the high-frequency limit.

Thus we have some justification for leaving the surface open in cases when it lies between the source and the observation points. An accurate open-surface numerical integration will compute the major contributing portion of the integrand on the exact infinite or closed surface.

B. Asymptotic Correction

Asymptotic analysis of the integral may also offer a correction that compensates in part for the missing portion. We rewrite the exact infinite integral in Eq. (13) as a sum of three integrals:

$$I = \left(\int_a^b + \int_{-\infty}^a + \int_b^{\infty}\right)F(y_1)\exp[-ik\psi(y_1)]\,dy_1 \tag{18}$$

The geometry is assumed to be such that the only stationary point of the integrand lies in $[a, b]$ and thus the first integral may be numerically computed and contains the major contribution to the value of I. Integration by parts is used to calculate asymptotic series in powers of $1/k$ for the second and third integrals:

$$\begin{aligned} I = {} & \int_a^b F(y_1)\exp[-ik\psi(y_1)]\,dy_1 - \exp[-ik\psi(a)] \\ & \times\left\{\frac{1}{k}\left[\frac{F(a)}{i\psi'(a)}\right] - \frac{1}{k^2}\left[\frac{F'(a)}{\psi'(a)^2} - \frac{F(a)\psi''(a)}{\psi'(a)^3}\right] + \frac{1}{k^3}(\cdots)\right\} \\ & + \exp[-ik\psi(b)]\left\{\frac{1}{k}\left[\frac{F(b)}{i\psi'(b)}\right]\right. \\ & \left. - \frac{1}{k^2}\left[\frac{F'(b)}{\psi'(b)^2} - \frac{F(b)\psi''(b)}{\psi'(b)^3}\right] + \frac{1}{k^3}(\cdots)\right\} \end{aligned} \tag{19}$$

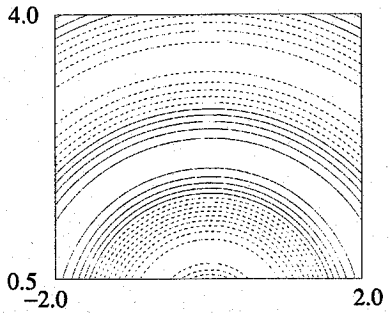

Fig. 3 Exact point source field (real part) for testing asymptotic end corrections. Contours: min = −0.015, max = 0.09, incr = 0.015; positive are solid, negative are dashed.

F may itself be a function of k, so it would not be correct to say that the next term in the series is $\mathcal{O}(1/k^3)$. The contributions at $\pm\infty$ are zero because of the decay of F with distance from the source. The end contributions are asymptotically small with respect to the contribution from the stationary point as $k \to \infty$, but for the finite k of an actual computation they offer a correction to the truncated integral.

C. Numerical Test of Correction Terms

To give insight into the effectiveness of these correction terms, we will perform a numerical experiment in two dimensions for the inhomogeneous reduced wave equation

$$(\Delta + k^2)\phi(\boldsymbol{x}) = \mathcal{S}(\boldsymbol{x}) \tag{20}$$

Our acoustic source will be a point monopole of unit strength at the origin. In the source notation of Eq. (8), $\mathcal{S}(z) = \delta(z)$. An exact solution field is plotted in Fig. 3. Our Kirchhoff surface (a line in this two-dimensional problem) will be positioned at $y_2 = h = 0.5$ and will extend from $y_1 = a = -2$ to $y_1 = b = 2$. The temporal wave number is $k = 2.5$, $kL = 10$. A simple calculation shows that the surface is 1.6 wavelengths long. Numerical integration in $[a, b]$ is performed with a simple fourth-order quadrature (Eq. 4.1.14 in Press et al.[13]). Errors are quantified with an L_1 error norm defined by

$$L_1 = \frac{\sum |\bar{\phi}_{ijk} - \phi_{ijk}|}{N_i N_j N_k} \tag{21}$$

where $\bar{\phi}$ is the exact solution, ϕ is the Kirchhoff result, and the summation is over all the calculated field points exterior to the Kirchhoff surface. The sum is normalized by the number of points in the summation. 300 points on the surface were used to evaluate the $[a, b]$ integral. Changing from 150 to 300 integration points resulted in a 0.005% change in the L_1 error norm, so the numerical integration is deemed highly accurate. All the terms in Eq. (19) are calculated analytically. The following is a table of L_1 error norms for inclusion of zero, one, and two correction terms (for reference, the norm of the exact solution calculated in a similar fashion over the same domain is 0.07423):

No. of corr. terms	L_1 error
0	0.00524
1	0.00129
2	0.00179

The error fields are plotted in Fig. 4. The error is defined as a simple difference between the exact and Kirchhoff solution.) Both the error-field plots and the L_1-norm data indicate that error is significantly reduced by the first end correction term and experiences a minor degradation for the choosen value of k when the second correction term is included. In our following study of a more realistic source, we will only consider the first term in the correction series, as it is the only term that seems to help at the moderate temporal wave numbers of interest and is easily calculated for general sources.

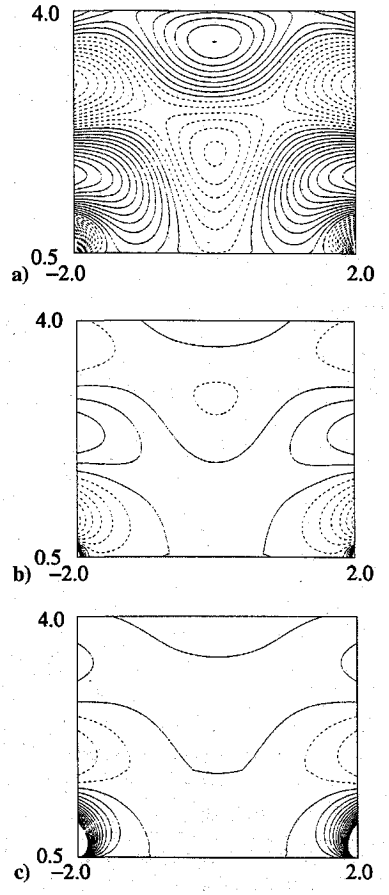

Fig. 4 Error fields (real part) for a) no end correction terms—contours: min = −0.015, max = 0.012, incr = 0.001; b) order-1/k end correction term only—contours: min = −0.006, max = 0.01, incr = 0.001; and c) order-1/k and 1/k^2 terms—contours: min = −0.003, max = 0.016, incr = 0.001. Positive contours are solid; negative contours are dashed.

We note here that the corrected solution is by far the poorest in the neighborhood of the endpoints (a, h) and (b, h). There are two reasons for this. The analysis leading to the corrected solution formula (19) uses asymptotic forms of the Hankel functions that are not applicable close to the endpoints. This would not present a problem in three dimensions, where it is possible to attain the phase of the fundamental solutions without relying on an asymptotic form. The technique presented in the next section will also not rely on asymptotic Hankel-function evaluation. A second cause for the poor performance in the vicinity of the endpoints is that the correction terms become singular. As $\boldsymbol{x} \to (a, h)$ or (b, h), the stationary point also approaches (a, h) or (b, h). This implies that $\psi'(a)$ or $\psi'(b) \to 0$. We see in Eq. (19) that the end corrections have ψ' in the denominator. Poor numerical performance is expected in the neighborhood of such a point. The L_1-error-norm improvements given in the above table would be more dramatic if the summation did not include points in the neighborhood of the endpoints.

Figure 5 shows the same error field as Fig. 4a, but the field calculation has been extended well beyond the Kirchhoff surface. We see that the solution degrades rapidly, consistent with the previous stationary-phase arguments, which showed that the major contribution to the integral value comes from the neighborhood of a point on the surface between the source and observation points. For points directly to the right and left of the surface, the stationary point is no longer included in the calculation and the solution is very poor. The correction terms do not help the solution in this situation, because they were derived on the premise that the stationary point lay within $[a, b]$.

For this same model problem and for a comparable problem in three spatial dimensions, Fig. 6 shows the behavior of the error vs the value of kL. The percentage error is defined as the L_1 error norm divided by the norm of the exact field. In two dimensions the amplitude of the exact solution has a $1/\sqrt{(kL)}$ dependence,

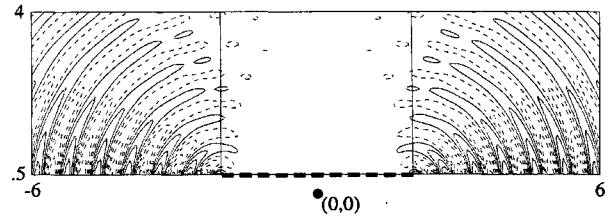

Fig. 5 Error field (real part) extended to the right and left of the Kirchhoff surface. The Kirchhoff surface is shown here with a heavy dashed line. The vertical lines indicate the region shown in Fig. 4a. Contours: min = −0.046, max = 0.046, incr = 0.0049. Positive contours are solid; negative contours are dashed.

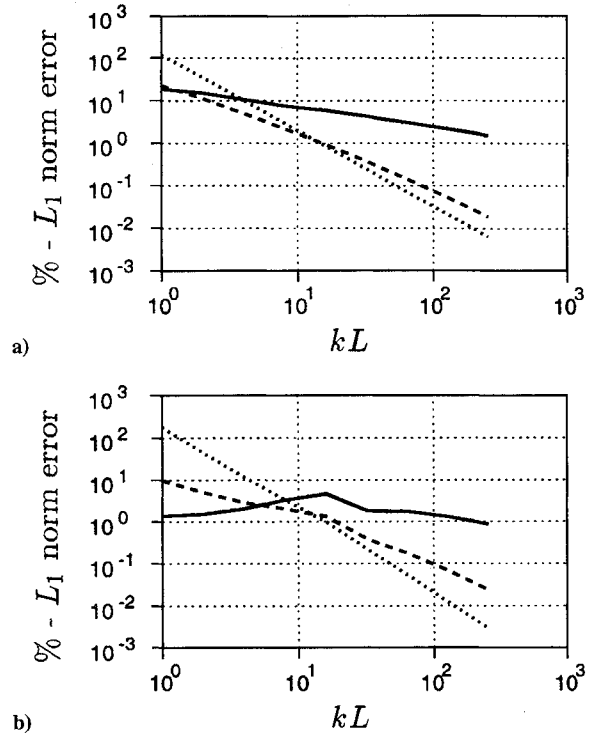

Fig. 6 Percentage error in the L_1 norm for zero (solid line), one (dashed line), and two (dotted line) correction terms. Here kL is the nondimensionalized temporal wave number: a) two-dimensional evaluation and b) three-dimensional evaluation.

and F in Eq. (19) is independent of kL. Therefore we expect the percentage error to have a $1/\sqrt{(kL)}$ dependence for zero correction terms, a $1/(kL)^{3/2}$ dependence when the first correction term is included, and a $1/(kL)^{5/2}$ dependence when the first and second correction terms are included. The zero- and one-correction-term cases do follow this behavior; the two-correction-term case does not, and this is because we took only the first term of the asymptotic form of the Hankel functions for large arguments. If we had included two terms,

$$H_n^{(2)}(k|\boldsymbol{x}|) \sim \left[e^{(\pi/4)i}\sqrt{\frac{2}{\pi k|\boldsymbol{x}|}} - e^{-(\pi/4)i}\frac{1}{8}\sqrt{\frac{2}{\pi k^3|\boldsymbol{x}|^3}} + \mathcal{O}\left(\frac{1}{(k|\boldsymbol{x}|)^{\frac{5}{2}}}\right)\right] \exp\left(in\frac{\pi}{2} - ik|\boldsymbol{x}|\right) \tag{22}$$

then $1/(kL)^{5/2}$ behavior would have been expected in Fig. 6a. However, with only the first Hankel term, there is an $\mathcal{O}[1/(kL)]$ error in F, which translates to an $\mathcal{O}[1/(kL)^2]$ error in the first correction term, so without a better approximation to the Hankel function we may never achieve better than $\mathcal{O}[1/(kL)^{3/2}]$ dependence for the percentage error [we have multiplied by $\mathcal{O}[\sqrt{(kL)}]$ to take account of the dependence of the exact the solution when calculating the percentage error]. In three dimensions the exact field norm is constant with kL, and F is $\mathcal{O}(kL)$. Therefore we expect the percentage error to have roughly $(kL)^n$ dependence, where n is the number of correction terms included from Eq. (19). This behavior is demonstrated in Fig. 6b.

D. Application to Real Sources

In a real application we do not know the form of $\mathcal{S}$, as we did in the previous numerical experiment where we specified a point source. Further analysis will be necessary to make end corrections in this case. Rewriting Eq. (12) in two dimensions with the $1/k$ end correction term gives

$$\phi(\boldsymbol{x}) = \int_{z\in\Omega_S}\left[\int_a^b F(y_1)\exp[-ik\psi(y_1)]\,dy_1 + \frac{F(b)\exp[-ik\psi(b)]}{ik\psi'(b)} - \frac{F(a)\exp[-ik\psi(a)]}{ik\psi'(a)} + \cdots\right] dz \tag{23}$$

The third dimension could be easily included. Distributing the z integration leads to the original Kirchhoff integral for an open surface $\partial\Omega_K$ plus two integral correction terms, one evaluated at each domain end. We take

$$\mathcal{A}(\boldsymbol{x};\boldsymbol{y}) = \phi(\boldsymbol{y})G_n(\boldsymbol{x}-\boldsymbol{y}) - \phi_n(\boldsymbol{y})G(\boldsymbol{x}-\boldsymbol{y}) \tag{24}$$

which consists of known terms, and arrive at the following, to order F/k:

$$\phi(\boldsymbol{x}) = \int_{y\in\partial\Omega_K}\mathcal{A}(\boldsymbol{x};\boldsymbol{y})\,dS(\boldsymbol{y}) + \int_{z\in\Omega_S}\left\{\frac{F(b;h,z,\boldsymbol{x})\exp[-ik\psi(b;h,z,\boldsymbol{x})]}{ik\psi'(b;h,z,\boldsymbol{x})} - \frac{F(a;h,z,\boldsymbol{x})\exp[-ik\psi(a;h,z,\boldsymbol{x})]}{ik\psi'(a;h,z,\boldsymbol{x})}\right\} dz \tag{25}$$

It is not possible to integrate the end correction terms exactly in z, because F/ψ' is an unknown function of z. Examining ψ' in Eq. (15), we see that the second term is independent of z. The first term depends upon z and in two dimensions is

$$\frac{y_1 - z_1}{\sqrt{(y_1-z_1)^2 + (y_2-z_2)^2}} \tag{26}$$

If $|\boldsymbol{z}-\boldsymbol{z}_0|$ is small, say $\approx\epsilon$, and $\epsilon \ll |\boldsymbol{y}|$, where $\boldsymbol{z}_0$ is an estimated point for the center of the sound source region Ω_S, then ψ' may be rewritten as a constant in z plus an error term:

$$\psi'(y_1; y_2, z, \boldsymbol{x}) = \frac{y_1 - z_{10}}{|\boldsymbol{y}-\boldsymbol{z}_0|} - \frac{x_1 - y_1}{|\boldsymbol{x}-\boldsymbol{y}|} + \mathcal{O}(\epsilon) \tag{27}$$

Once this approximation is made, the integrals in z for the end corrections terms may be evaluated, and the result is

$$\phi(\boldsymbol{x}) = \int_{y\in\partial\Omega_K}\left[\mathcal{A} + \frac{\mathcal{A}(b)}{ik\psi'(b)} - \frac{\mathcal{A}(a)}{ik\psi'(a)} + \mathcal{O}(\epsilon)\right] dS(\boldsymbol{y}) \tag{28}$$

Whether or not it is possible to estimate $\boldsymbol{z}_0$ and have Ω_S, the region of source support, be small enough for the above approximation to be valid depends upon the particular flow in the source calculation. Considering the axisymmetric jet calculation of Mitchell et al.,[3] we see that the source location in that case may be defined fairly precisely—it is the location of the vortex pairing. Mitchell et al. also determined that for their jet the Kirchhoff surface needed to be 10 jet radii away from the jet centerline. If the computational box extends more than 10 radii downstream and we assume that the region of noise generation is approximately 1 radius in extent, then we have a condition that $\epsilon/|\boldsymbol{y}| \approx 0.1$. A sample calculation is performed using a model source of similar extent in the next section, and the results are excellent.

If the flow is such that the above approximation will not be valid (e.g., a case where one cannot determine the position of the source for a particular temporal wave number k), one must seek other means of estimating ψ'. For example, the local phase may be estimated by calculating the distance between zero crossings of the integrand. The local-phase estimates could then be finite differenced to give an estimate of the phase slope at points a and b.

Note that the form of solution presented in Eq. (25) is exactly the same for two and three dimensions, the only difference being the number of integrations necessary. If there were a finite mean flow parallel to the x_1 direction (as there would be for a jet with coflow or a mixing layer), the form of ψ' would change, but Eq. (25) would still hold. The y_1 derivative of the phase for nonzero mean flow in two dimensions is

$$\psi'(y_1) = -\left[\frac{(y_1 - z_1)^2}{1 - M^2} + (y_2 - z_2)^2\right]^{-\frac{1}{2}} \frac{y_1 - z_1}{(1 - M^2)^{\frac{3}{2}}}$$

$$+\left[\frac{(x_1 - y_1)^2}{1 - M^2} + (x_2 - y_2)^2\right]^{-\frac{1}{2}} \frac{(x_1 - y_1)}{(1 - M^2)^{\frac{3}{2}}} \tag{29}$$

The extension to three dimensions is exactly analogous. A nonzero mean flow is considered for an example calculation presented in the next section.

E. Sample Calculation for Model Source

In this section the source-location estimation technique discussed in the previous section is applied to a source of finite extent. We let the convected reduced wave equation (5) with source

$$S(z) = 100 \exp\left(-33z_1^2 - 129z_2^2\right) \tag{30}$$

govern the radiated field. This gives $S(z) \approx 0.25S(0)$ for $z = (0.2, 0)$ and at $z = (0, 0.1)$, which is approximately the size of the source region for the first vortex pairing event in an axisymmetric jet. S decays to 10^{-14} by $z = (1, 0)$ and $z = (0, 0.5)$. The position of the surface is chosen to mimic the position in an actual source-flow calculation: $h = 0.5$, $a = 2$, $b = -2$. We take $k = 10$, giving $kL = 40$. The mean flow is taken to be $M = 0.5$ and in the x_1 direction. The values of $\phi(y)$ on the surface were computed by performing the convolution in Eq. (8). The normal derivative $\phi_n(y)$ was calculated by finite-differencing two closely spaced $\phi(y)$ convolution results. Decreasing this spacing had a negligible effect on the resulting normal-derivative calculation. Quadrature was performed using the same fourth-order method as in Sec. III.C. In each coordinate direction, 25 points are used to evaluate the two-dimensional convolution integral. Using 50 points in each direction resulted in less than a 0.001% change in the results for the field. The values of $\phi(x)$ in the sound field was calculated using the same convolution integral and were used to evaluate the Kirchhoff calculations with and without the end corrections. 150 quadrature points were used in evaluating the Kirchhoff integral on $[a, b]$. The L_1 error norms are again calculated and are presented here (for reference, the norm of the field as calculated by the convolution integral is 0.107927):

No. of corr. terms	L_1 error
0	0.003034
1	0.000199

That this result represents a better improvement than calculated in the point-source calculation of Sec. III.C is believed to be a result of better performance in the vicinity of the endpoints. This solution relies less on the asymptotic form of the Hankel functions. The exact solution is plotted in Fig. 7. The noncompactness of the source gives the radiated field a directivity more complex than a point monopole source in the same flow. Error fields for zero and one correction term are plotted in Fig. 8. We see a drastic reduction in the overall error with the inclusion of the end correction. The large value of kL was chosen to give an interesting directivity. The accuracy trends as a function of kL are analogous to the one-correction-term case shown for the point monopole source in Fig. 6.

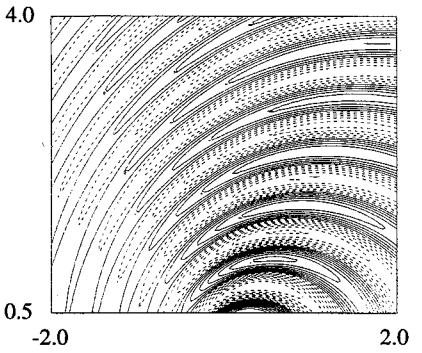

Fig. 7 Convolution field (real part) for source given in Eq. (30). Contours: max = 0.28, min = −0.23, incr = 0.033; positive are solid, negative are dashed.

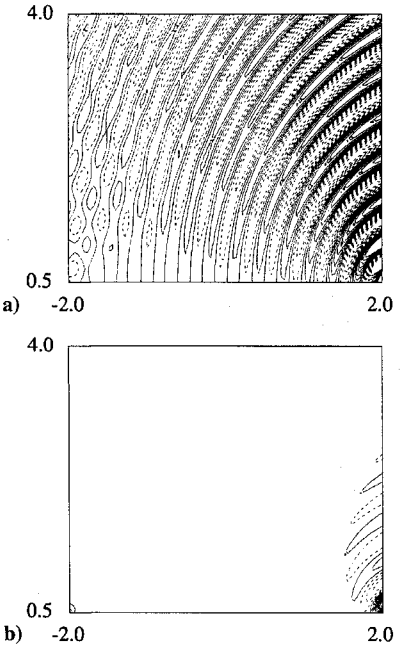

Fig. 8 Error fields (real part) for Kirchhoff evaluation of Eq. (30) field: a) no end correction terms—contours: min = −0.01, max = 0.01, incr = 0.001 and b) order-1/k correction term—contours: min = −0.0035, max = 0.01, incr = 0.001. Positive contours are solid; negative contours are dashed.

IV. Time-Domain Formulation

The analysis completed thus far has assumed a time-harmonic sound field with temporal dependence $e^{+i\omega t}$. The analysis may be extended to a time-dependent situation by converting results back to the time domain directly. We take $\tilde{\phi}(x, t)$ to be a time-dependent field variable. Time-harmonic terms having factors of $i\omega$ indicate differentiation in the time domain:

$$i\omega \rightarrow \frac{\partial}{\partial t} \tag{31}$$

and terms containing factors of $1/i\omega$ indicate integration in the time domain:

$$\frac{1}{i\omega}\hat{\phi}(y) \rightarrow \int_{-\infty}^{t} \tilde{\phi}(y, \tau)\, d\tau \tag{32}$$

where the $-\infty$ may be replaced by a time in the past before which there is no sound. Used in conjunction with a flow calculation, this would correspond to the beginning of the simulation. Retarded times enter the problem though the following conversion:

$$\hat{\phi}(y) \exp(-ik|x - y|) \rightarrow \tilde{\phi}\left(y, t - \frac{|x - y|}{c}\right) \tag{33}$$

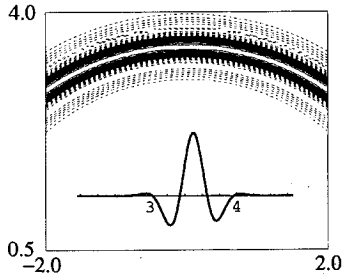

Fig. 9 Exact field for source given in Eq. (36). Contours: max = 0.023, min = −0.011, incr = 0.0018; positive are solid, negative are dashed. The inset plot is the exact field value vs $|x|$ for the same field equation.

Applying the above conversions to Eq. (28) formulated in three dimensions and defining

$$\mathcal{B} = \tilde{\phi}\left(\mathbf{y}, t - \frac{R}{c}\right)\frac{\boldsymbol{R}\cdot\boldsymbol{n}}{4\pi R^3} + \frac{\boldsymbol{R}\cdot\boldsymbol{n}}{4\pi R^2 c}\frac{\partial\tilde{\phi}}{\partial t} - \frac{\partial\tilde{\phi}}{\partial n}\frac{1}{4\pi R} \tag{34}$$

to simplify expressions, we arrive at the following expression for the time-dependent Kirchhoff formulation with end correction terms:

$$\tilde{\phi}(\boldsymbol{x}, t) = \int_{y\in\partial\Omega_K}\left[\mathcal{B}\left(\mathbf{y}, t - \frac{R}{c}; \boldsymbol{x}\right)\right.$$
$$+ \frac{c}{\psi_0'(b)}\int_{-\infty}^{t-R/c}\mathcal{B}(\mathbf{y}, \tau; b)\,\mathrm{d}\tau$$
$$\left. - \frac{c}{\psi_0'(a)}\int_{-\infty}^{t-R/c}\mathcal{B}(\mathbf{y}, \tau; a)\,\mathrm{d}\tau\right]\mathrm{d}S(\mathbf{y}) \tag{35}$$

$\boldsymbol{R}$ is defined by $\boldsymbol{R} = \boldsymbol{x} - \mathbf{y}$, and $R = |\boldsymbol{R}|$. The end corrections now appear as time-history integrations starting at a quiet time in the past and ending at the retarded time for the given observation point. The first term in the surface integral is the standard Kirchhoff integrand for time-dependent problems and is well known.[5]

We again evaluate performance with a numerical experiment for a model source and choose the exact sound field in three dimensions:

$$\tilde{\phi}(\boldsymbol{x}, t) = \frac{1}{4\pi|\boldsymbol{x}|}\cos\left(\omega\frac{t-|\boldsymbol{x}|}{c}\right)\exp\left[-\sigma\left(\frac{t-|\boldsymbol{x}|}{c}\right)^2\right] \tag{36}$$

where σ is a parameter dictating the width of the Gaussian envelope. Numerical values are assigned to the parameters: $\omega = 1.0, \sigma = 0.1$, and $c = 0.1$, and for the example given, we take the present time $t = 35$. A contour and line plot of the exact wave field is given in Fig. 9. The Kirchhoff surface is that shown in Fig. 2 with $a = -2$ and $b = 2$ as before. The y_1 integration is performed exactly as before. The numerical time-history integrations for the correction terms are performed with the same fourth-order quadrature discussed in Sec. III.C. A spectral method is used to calculate the θ-direction integration necessary for this three-dimensional problem. 101 points were used in the y_1 integration, and 32 in the θ integration. Switching to 202 in y_1 and 48 in θ resulted in a 0.06% change in the L_1 norm of the uncorrected field. 50 points were used for the temporal integration of the end correction terms. Changing from 50 to 100 points resulted in a 0.02% change the L_1 norm of the end correction field. The norm of the uncorrected field pictured in Fig. 9 is 0.0024792, and the error fields for zero and one correction term are given in the table below:

No. of corr. terms	L_1 error
0	0.0001281
1	0.0000340

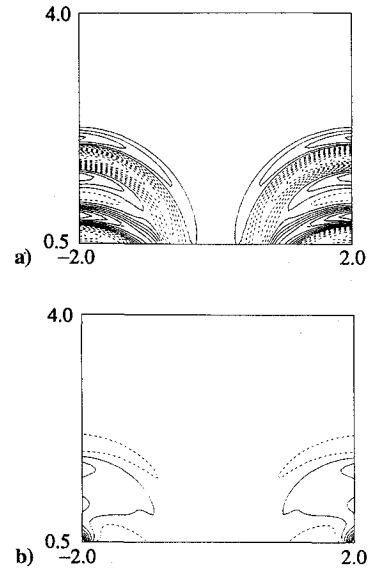

Fig. 10 Error fields for time-domain Kirchhoff evaluation of Eq. (36) field: a) no end correction terms and b) with end correction term. Contours (both plots): min = −0.0014, max = 0.0012, incr = 0.00014. Positive contours are solid; negative contours are dashed.

We see nearly a factor-of-4 reduction of the error with inclusion of the end corrections. Error fields for the straight Kirchhoff surface evaluation and the corrected evaluation are shown in Fig. 10. The error in the vicinity of points (a, h) and (b, h) is believed due, as before, to the singular nature of the correction terms at these points. Generally, one would be interested in points further away from the source flow. Leaving the local endpoint regions out of the L_1-norm calculations above would show a more dramatic improvement resulting from the end corrections.

V. Conclusions

Stationary phase analysis of the Kirchhoff integral has demonstrated that the major contribution comes from a point on the surface that intersects a line between the observation and the source point. If acoustic data are available on an open Kirchhoff surface lying between the observation point and all possible source locations, then we may calculate the major contribution to the integral by numerically integrating over this open surface. It is found that flows of interest have values of the temporal wave number for which application of this rule gives reliable results.

Asymptotic methods were also used to analyze the unavailable portions of the integrals and provide a correction to the open integral representing the unavailable portions. This correction was found to reduce the error by more than a factor of 10 in a model problem. The analysis was extended to time-domain problems, and again a significant reduction of error is accomplished with inclusion of end corrections.

Acknowledgments

This work was sponsored by the Office of Naval Research, Grant N00014-92-J-1626. We thank Joseph Keller for helpful discussions.

References

[1]Lyrintzis, A. S., "Review: The Use of Kirchhoff's Method in Computational Aeroacoustics," *Journal of Fluids Engineering*, Vol. 116, No. 4, 1994, pp. 665–676.

[2]Kirchhoff, G. R., "Toward a Theory of Light Rays," *Annals of Physical Chemistry*, Vol. 18, 1883, pp. 663–695.

[3]Mitchell, B. E., Lele, S. K., and Moin, P., "Direct Computation of the Sound Generated by Vortex Pairing in an Axisymmetric Jet," AIAA Paper 95-0504, 1995.

[4]Lyrintzis, A. S., and Mankbadi, R. R., "On the Prediction of the Far-Field Jet Noise Using Kirchhoff's Formulation," AIAA Paper 95-0508, 1995.

[5]Pierce, A. D., *Acoustics: An Introduction to its Physical Principles and Applications*, Acoustical Society of America, New York, 1989.

[6]Schenck, H. A., "Improved Integral Formulation for Acoustic Radiation Problems," *Journal of the Acoustical Society of America*, Vol. 44, No. 1, 1967, pp. 41–58.

[7]Abramowitz, M., and Stegun, I. A., *Handbook of Mathematical Functions*, Dover, New York, 1965.

[8]Wu, T. W., and Lee, L., "A Direct Boundary Integral Formulation for Acoustic Radiation in a Subsonic Uniform Flow," *Journal of Sound and Vibration*, Vol. 175, No. 6, 1993, pp. 51–63.

[9]Howe, M. S., "The Influence of Vortex Shedding on the Generation of Sound by Convected Turbulence," *Journal of Fluid Mechanics*, Vol. 76, No. 4, 1976, pp. 711–740.

[10]Farassat, F., and Myers, M. K., "Extension of Kirchhoff's Formula to Radiation from Moving Surfaces," *Journal of Sound and Vibration*, Vol. 123, No. 3, 1988, pp. 451–460.

[11]Colonius, T., Lele, S. K., and Moin, P., "Direct Computation of the Sound Generated by a Two Dimensional Shear Layer," AIAA Paper 93-4328, 1993.

[12]Lax, M., and Feshbach, H., "On the Radiation Problem at High Frequencies," *Journal of the Acoustical Society of America*, Vol. 19, No. 4, 1947, pp. 682–690.

[13]Press, W. H., Flannery, B. P., Saul, A. T., and Vetterling, W. T., *Numerical Recipes*, Cambridge Univ. Press, New York, 1988.